nature geoscience

ARTICLES

https://doi.org/10.1038/s41561-021-00695-3

Projections of tropical heat stress constrained by atmospheric dynamics

Yi Zhang[1]✉, Isaac Held[1] and Stephan Fueglistaler[1,2]

Extreme heat under global warming is a concerning issue for the growing tropical population. However, model projections of extreme temperatures, a widely used metric for extreme heat, are uncertain on regional scales. In addition, humidity needs to be taken into account to estimate the health impact of extreme heat. Here we show that an integrated temperature–humidity metric for the health impact of heat, namely, the extreme wet-bulb temperature (TW), is controlled by established atmospheric dynamics and thus can be robustly projected on regional scales. For each 1 °C of tropical mean warming, global climate models project extreme TW (the annual maximum of daily mean or 3-hourly values) to increase roughly uniformly between 20° S and 20° N latitude by about 1 °C. This projection is consistent with theoretical expectation based on tropical atmospheric dynamics, and observations over the past 40 years, which gives confidence to the model projection. For a 1.5 °C warmer world, the probable (66% confidence interval) increase of regional extreme TW is projected to be 1.33–1.49 °C, whereas the uncertainty of projected extreme temperatures is 3.7 times as large. These results suggest that limiting global warming to 1.5 °C will prevent most of the tropics from reaching a TW of 35 °C, the limit of human adaptation.

The impact of global warming on local extreme heat is projected to be detectable earliest in the tropics[1–3], where baseline temperatures are already high. In addition, countries located between 20° S and 20° N latitude will soon become major contributors to the global population growth[4], and there is thus a pressing need for accurate projections of extreme heat in the tropics down to regional scales.

The most widely used metric for extreme heat has been the extreme temperature. However, projections of extreme temperatures have large regional uncertainty arising from insufficient model representation of important land processes[5]. Moreover, to facilitate the estimation of heat-induced health impact (or heat stress), the effect of humidity should also be included[6,7]. This is because the major way for humans to lose metabolic heat in hot weather is evaporative cooling (sweating)[8,9], the efficiency of which anti-correlates with humidity. In particular, the inclusion of humidity is necessary for assessing heat stress in the tropics, the warmest and the most humid places on Earth.

The importance of humid heat has been increasingly recognized[10,11]. Studies have shown that increased humidity with temperature following the Clausius–Clapeyron relationship can worsen summer heat stress in the tropics[12,13], while other work has noticed a reduction in either relative humidity[14] or specific humidity[15] on the hottest days (not limited to the tropics). Given the possibility that humidity can interact with temperature in extreme heat, it is necessary to better quantify and improve our mechanistic understanding for the control of humid heat.

Here, we use the extreme wet-bulb temperature (TW), an integrated temperature–humidity metric for heat stress (Methods). TW by definition is the lowest temperature that human skin can be cooled to through evaporation of sweat. Therefore, the closer TW is to the upper limit of human skin temperature (around 35 °C), the more intolerable the heat is, with a survival limit of TW = 35 °C (ref. [16]) (high TW values below this survival limit also have adverse health impact). Furthermore, TW is a major component in the wet-bulb globe temperature (WBGT; Methods)[17], which is the standard metric for workplace heat stress. In this article, we argue that the regional extreme TW in the tropics is controlled mainly by robust atmospheric dynamics that have been established previously[18–21], rather than by local processes that are more uncertain. Therefore, tropical extreme TW can be robustly projected on regional scales under global warming.

Global climate model projections

Figure 1a shows the projections of extreme TW (TW_{max}) and extreme temperatures (T_{max}) by 22 global climate models (Supplementary Table 1) from the Coupled Model Intercomparison Project phase 5 (CMIP5)[22] under the representative concentration pathway 8.5 (RCP 8.5) emission scenario (TW_{max} and T_{max} refer mostly to the annual maximum of daily mean values in this paper and refer to the annual maximum of 3-hourly values when specifically stated). The multi-model mean of T_{max} averaged over tropical land within 20° S–20° N warms faster than the tropical mean temperature. However, TW_{max} closely follows the tropical mean warming, similar to an earlier finding using an atmospheric model coupled to a slab ocean[16]. These results also hold when analysing 3-hourly data that resolve the diurnal cycle from two models (GFDL-CM3 and IPSL-CM5A-LR) (Fig. 1b,c).

Figure 1d,e shows T_{max} and TW_{max} trends for all locations normalized by the tropical mean warming under RCP 8.5. T_{max} warming is spatially inhomogeneous over land ranging from 1.0 °C to 2.3 °C for each 1 °C of tropical mean warming (Fig. 1d), consistent with previous findings. By contrast, we find that increases of TW_{max} have no notable land–ocean contrast ranging from 0.8 °C to 1.3 °C for each 1 °C of tropical mean warming (Fig. 1e). Using the annual-maximum 3-hourly TW for TW_{max} does not change this result (Supplementary Fig. 1).

The spatially uniform TW_{max} trend (Fig. 1e) is not a cancellation of errors among different models. Instead, all models show good agreement on TW_{max} trend, even down to regional scales. Fig. 2 shows the model spread (2.5–97.5th percentiles) of T_{max} and TW_{max} projections for four selected regions that have caught substantial

[1]Program in Atmospheric and Oceanic Sciences, Princeton University, Princeton, NJ, USA. [2]Department of Geosciences, Princeton University, Princeton, NJ, USA. ✉e-mail: yz8@princeton.edu

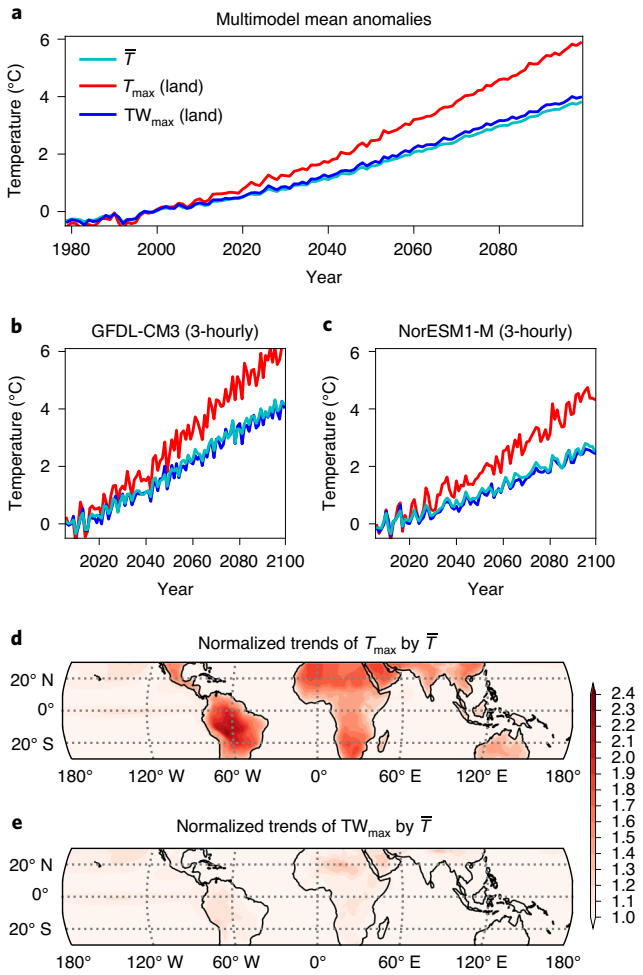

Fig. 1 | TW_{max} and T_{max} trends in climate models under RCP 8.5. a, Multimodel-mean time series of the tropical mean (20° S–20° N) temperature ($\overline{T}$; cyan), land-mean T_{max} (red) and land-mean TW_{max} (blue). **b**,**c**, The same as **a** but using the annual-maximum 3-hourly values for T_{max} and TW_{max} for two individual models. **d**,**e**, Multimodel-mean location-specific T_{max} and TW_{max} trends normalized by $\overline{T}$ trends.

attention in the literature: the Amazon rain forest, the Maritime Continent, the Indian peninsula and the Sahel. The projected T_{max} warming has large spread among models, which is especially prominent in the Amazon rain forest, consistent with earlier analysis[5]. However, for regional TW_{max}, all 22 climate models project a close to 1/1 ratio with the tropical mean warming. Using the annual maximum of 3-hourly TW does not change this result (Supplementary Fig. 2). Intriguingly, the model spread of T_{max} tends to grow with the amplitude of the projected warming (pronounced for the Amazon rain forest and the Maritime Continent), whereas the model spread of TW_{max} does not show evident growth within the range of simulated warming (roughly 4 °C). That the intermodel spread is much less for TW_{max} projections than for T_{max} is also true for other tropical land regions (Supplementary Fig. 3).

To summarize, global climate models predict that TW_{max} will increase roughly uniformly in the tropics by about 1 °C for each 1 °C of tropical mean warming. Models show wide spread on regional T_{max} projections but agree very well upon regional TW_{max}.

Theoretical support

For a theoretical projection of TW_{max}, we argue that tropical atmospheric dynamics exert a strong, tropics-wide control on local TW_{max}. This control is through the functional relationship between TW and moist static energy (MSE; Supplementary Fig. 4), which is a variable regulated by atmospheric dynamics. In the tropics, the free-tropospheric temperature is roughly uniform in the horizontal as a result of the weak effect of the Earth's rotation. This horizontally uniform temperature, which is determined by the near-surface MSE in regions of deep convection, sets the upper bound for MSE at all locations. Indeed, the maximum near-surface MSE is roughly uniform within 20° S–20° N (even more uniform than the time-mean MSE; Supplementary Fig. 5a,b), and the spatial pattern of TW_{max} closely follows the uniformity of the maximum MSE (Supplementary Fig. 5c). As this upper bound for near-surface MSE and, equivalently, for TW is a common one over land or over ocean[21], we expect that changes in TW_{max} should also be roughly equal over land and over ocean under global warming:

$$\Delta TW_{max,Land} \approx \Delta TW_{max,Ocean} \quad (1)$$

Equation (1) thus provides a handle on TW_{max} over land which is challenging to predict due to various land types and land processes, as a theoretical projection for TW_{max} over ocean can be made relatively easily. Near the ocean surface, air is close to saturation and TW changes are approximately equal to temperature changes (exactly equal when air is saturated); $\Delta TW_{max,Ocean}$ is thus approximately equal to the change in the warmest sea surface temperatures (SSTs). Therefore, 1 °C of $\Delta TW_{max,Land}$ is accompanied by 1 °C of warming of the warmest SSTs according to Eq. (1). Furthermore, the area dominance of the ocean and the relatively constant shape of SST histogram under global warming (Supplementary Fig. 6) together result in a 1/1 correspondence between warming of the warmest SSTs and the tropical mean temperature. (While there is potential for differences between changes in these relatively warm SSTs and the tropical mean SST[23–25], we find these differences to be small enough that they do not undermine the theoretical considerations here.) We thus expect $\Delta TW_{max,Land}$ roughly equals the tropical mean warming.

Global climate models shown in Figs. 1 and 2 are consistent with the preceding theoretical considerations. For each 1 °C of tropical mean warming, models on average give 1.05 °C of $\Delta TW_{max,Land}$, 0.93 °C of $\Delta TW_{max,Ocean}$ and 0.91 °C of the warmest-quartile-mean SST increase, all close to 1 °C.

The non-local control of TW_{max} by the warmest SSTs seems to be at odds with the perception that these extreme events are driven by rare local meteorology, and this controversy deserves some clarification. While TW_{max} events are driven by local processes, the potential magnitude of TW_{max} is largely set by the uniform free-tropospheric temperature. The effectiveness of this non-local control is evident in the uniformity of TW_{max} increases in Fig. 1e and the good agreement across models in Fig. 2, neither of which can be explained by the heterogeneity of local processes. Moreover, the existence of such a non-local control within the tropics also explains why the tropics are consistently warm and humid, but the highest TW and WBGT are observed in the subtropics[13,26,27]. These considerations thus support the picture that the magnitude of ΔTW_{max} across tropical land regions is set by the warmest SSTs and not by local processes or the spatial pattern of SST.

Observational evidence

From 1979 to 2018, the tropical (20° S–20° N) land-mean T_{max} trend has a 95% confidence interval of 0.24–0.31 °C per decade, which is almost three times the tropical mean warming of 0.08–0.12 °C per decade on the basis of the European Centre for Medium-Range Weather Forecasts Reanalysis Interim (ERA-Interim)[28] (Fig. 3a). TW_{max} has a trend of 0.05–0.10 °C per decade, very similar to the tropical mean warming, and the interannual variabilities of the two are highly correlated, with a correlation coefficient of 0.85 (Fig. 3a). Using the annual-maximum 3-hourly TW from ERA-Interim yields

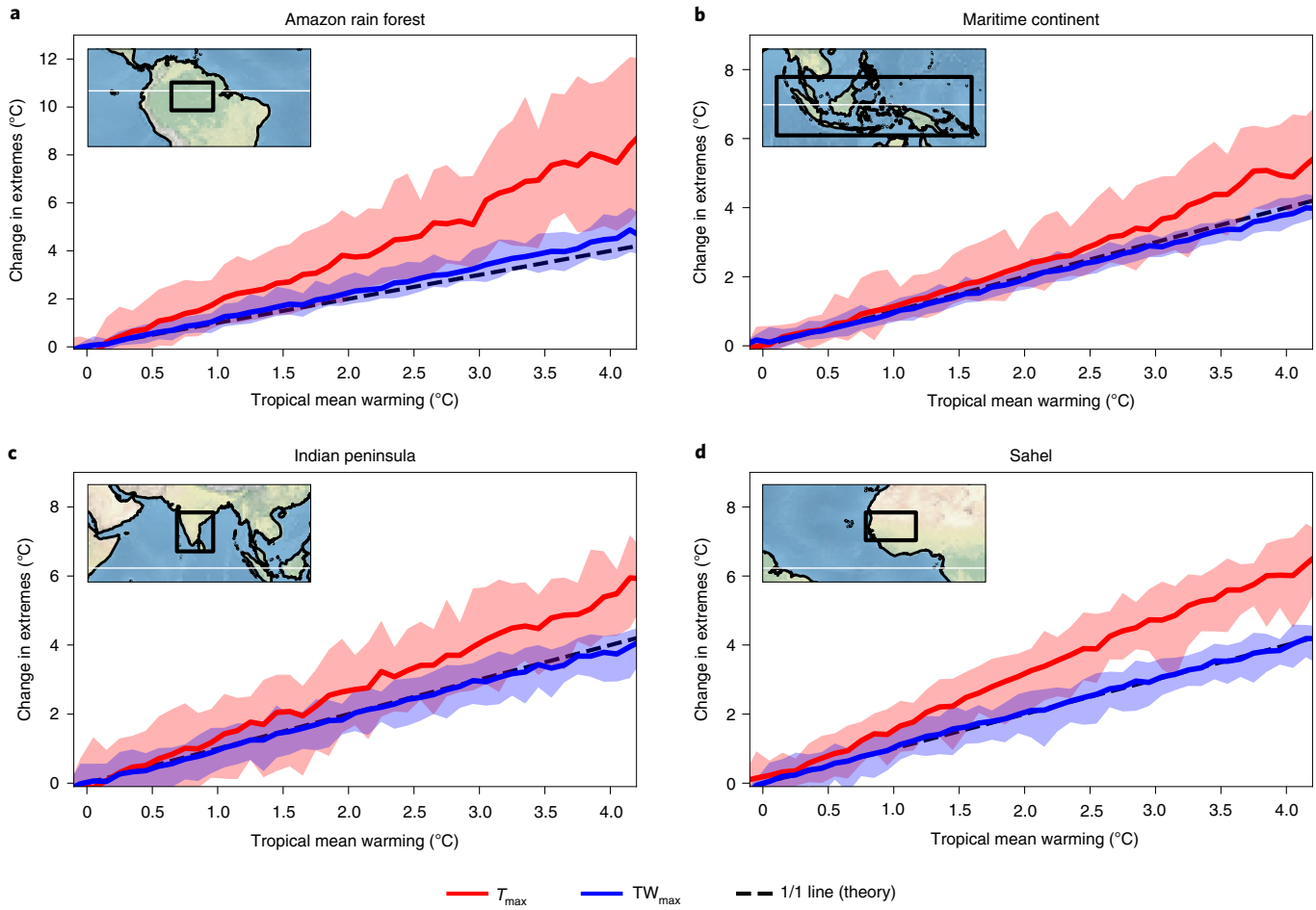

Fig. 2 | Model agreement on regional TW_{max} projections. a–d, Multimodel means (lines) and spreads (2.5–97.5th percentiles; shading) for regional T_{max} (red) and TW_{max} (blue) as a function of the tropical mean warming are shown for four regions: Amazon rain forest (**a**), Maritime Continent (**b**), Indian peninsula (**c**) and Sahel (**d**). Only land data within the black frames on the maps are sampled. The dashed black lines indicate the 1/1 ratio.

very similar anomalies, although the long-term trend is smaller (Supplementary Fig. 7). Furthermore, station measurements of TW provided by HadISD[29] (Methods and Supplementary Fig. 8) show that TW_{max} averaged over tropical stations is highly correlated with that from ERA-Interim and has a similar trend of 0.05–0.10 °C per decade (Fig. 3a). The consistency of reanalysis data with station observations and the theory lends support to the quality of the reanalysis data over tropical land.

The warmest-quartile-mean SST (the average of the top 25% of monthly SST at all grid points within each year) from HadISST[30] is highly correlated with land-mean TW_{max} and has a similar trend of 0.08–0.12 °C per decade (Fig. 3a). Satellite SST observations and station TW observations are largely independent, and the very good consistency in their extreme values lends strong support to the aforementioned argument that TW_{max} over land is coupled to the warmest SSTs. Strong El Niño events have the potential of warming the warmest SSTs and, as a result, affect TW_{max} over land (for example, 1998 in Fig. 3a).

Location-specific evaluation of long-term TW_{max} trends for the observations suffers from the smallness of the warming signal, but interannual variability of SST provides room for testing the 1/1 relationship with TW_{max}. Regression slopes of TW_{max} (ERA-Interim) onto the tropical mean temperature (linear trends removed) is relatively uniform over most of the land regions within 20° S–20° N (Fig. 3b) with a mode value very close to 1 (Fig. 3c). This relationship loosens in the subtropics (indicated by the hatching in Fig. 3b), consistent with the latitudinal range where the theory works[21]. That the Andes and the southern edge of the Sahara have much higher TW_{max} sensitivity does not violate the proposed theory, as climatological TW_{max} in those regions is too low to trigger convection and thus not constrained by the aforementioned mechanism. The standard deviation of these slopes in the reanalysis is larger than that for the global warming simulations shown in Fig. 1e (Fig. 3c). A likely explanation is that the spatial pattern of TW_{max} can change in the interannual variability, and such a spatial rearrangement can cause a spread in the regression slopes but does not affect the tropical averages shown in Fig. 3a. Indeed, global climate models also show a similar spread of TW_{max} trends under historical radiative forcing, and the removal of long-term trends in the global warming simulations for the same set of models also results in a similar spread (Fig. 3c). Therefore, regional TW_{max} trends diagnosed from reanalysis data over the past 40 years are consistent with global climate models. For similar reasons, we do not expect every station to give the same TW_{max} trend.

While we do not attempt to formulate an attribution statement for the TW_{max} trend over land seen in Fig. 3a, we note that the tight relationship in the overall trend as well as higher frequency variability strongly suggests that any attribution statements for the tropical mean temperature or SST can also be applied to TW_{max}.

Implications for the future climate

Consistency of model results with the theory and observations lends strong support to the capability of global climate models in properly simulating regional TW_{max} increases. In a 1.5 °C warmer

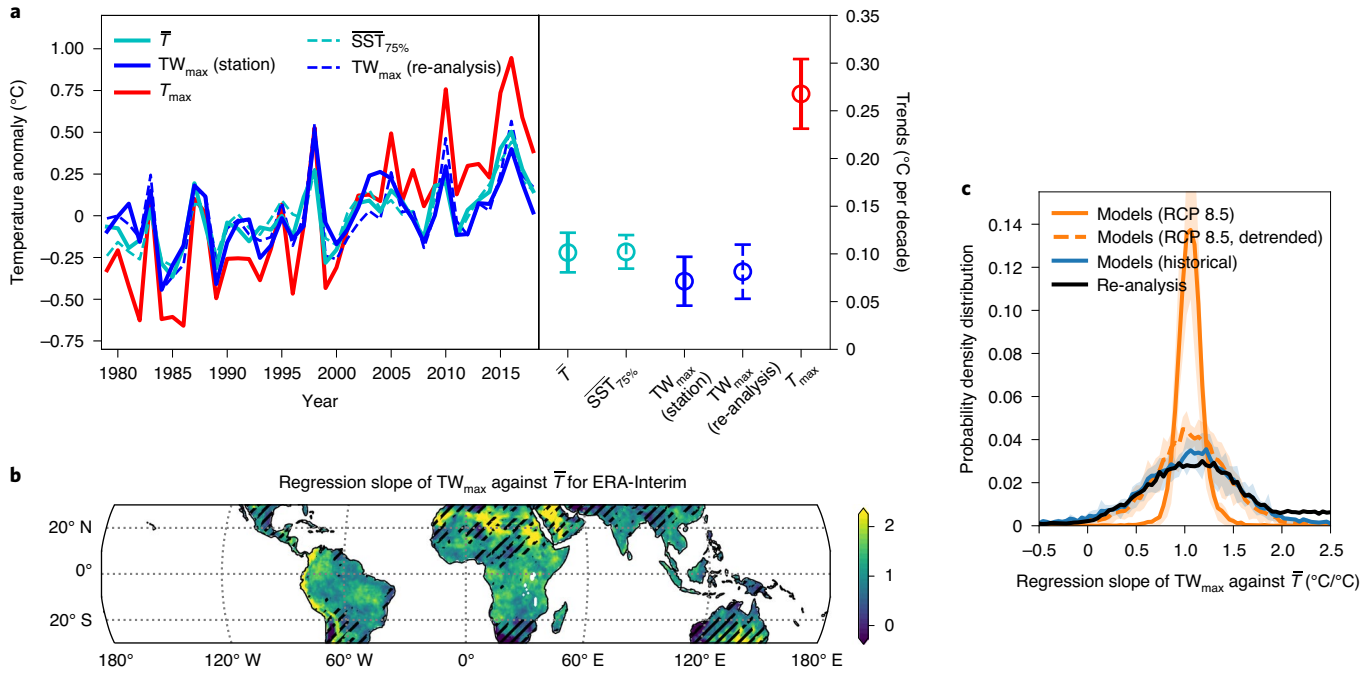

Fig. 3 | TW_{max} in observations and reanalysis data. a, Time series and corresponding linear trends of tropical mean temperature ($\overline{T}$; solid cyan), land-mean T_{max} (red), land-mean TW_{max} from stations (solid blue) and ERA-Interim (dashed blue), and the warmest-quartile-mean SST from HadISST (dashed cyan) for 1979–2018 (20° S–20° N). The confidence intervals for the linear trends represent 95% significance assuming that the detrended annual data points are independent. **b**, Linear regression slopes of local TW_{max} onto $\overline{T}$ in the interannual variabilities (linear trends removed) from ERA-Interim for 1979–2018. Regions where TW_{max} and $\overline{T}$ are not correlated on a 95% significance level are hatched. **c**, Histograms of regression slopes of local TW_{max} onto $\overline{T}$ (linear trends removed) for 1979–2005 in ERA-Interim (black solid) and models (blue solid) and for the global warming simulations in models (orange dashed). The same histogram for non-detrended global warming simulations (Fig. 1e) is also shown (orange solid). Shading indicates the 25–75th percentiles of models.

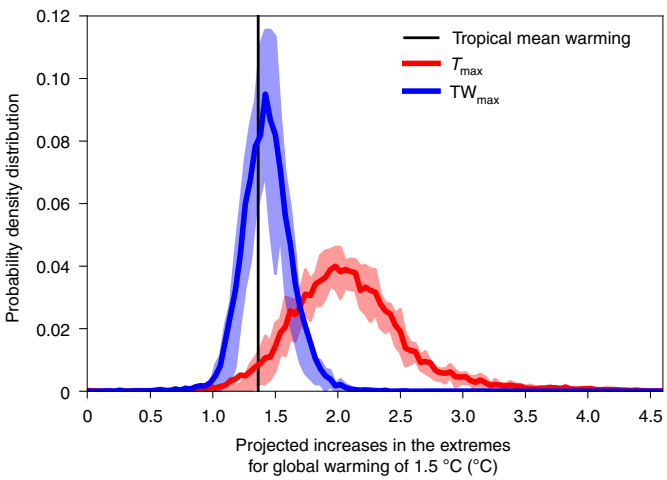

Fig. 4 | Uncertainty of T_{max} and TW_{max} projection in a 1.5 °C warmer world (land between 20° S and 20° N). Distributions of model-projected TW_{max} increases (blue) and T_{max} increases (red) under RCP 8.5 at 1.5 °C of global mean warming are shown. The distributions are constructed by linearly regressing local T_{max} and TW_{max} increases onto global mean warming and taking the regression values at 1.5 °C of global mean warming. Solid lines show the average distribution of all models, and the shading indicates the 25–75th percentiles across models.

world, the projected 66% confidence interval (equivalent to the Intergovernmental Panel on Climate Change's 'likely range') for TW_{max} increases across all tropical land regions (20° S–20° N) is 1.33–1.49 °C, consistent with the simulated tropical mean warming of ~1.4 °C in a 1.5 °C warmer climate (Fig. 4). However, projected T_{max} increases have a wider distribution, the absolute (relative) standard deviation of which is 3.7 (1.8) times that of TW_{max} increases. The reduction in uncertainty is more pronounced for regions where T_{max} projections are most uncertain. For example, in the Amazon rain forest and the Maritime Continent (Fig. 2), the absolute (relative) uncertainty of T_{max} increases is around 4 (2.5) times that of TW_{max} increases.

Our results imply that curtailing global mean warming will have a proportional effect on regional TW_{max} in the tropics. The maximum 3-hourly TW (ERA-Interim) ever experienced in the past 40 years by 99.98% of the land area within 20° S–20° N is below 33 °C. Therefore, a 1.5 °C or 2 °C warmer world will likely exempt the majority of the tropical area from reaching the survival limit of 35 °C. However, there exists little knowledge on safety thresholds for TW besides the survival limit[11], and 1 °C of TW increase could have adverse health impact equivalent to that of several degrees of temperature increase. TW will thus have to be better calibrated to health impact before wider societal implementation. Nonetheless, the confidence in TW_{max} projection provided in this work still raises the confidence in the projections of other calibrated heat stress metrics that account for TW, such as the WBGT.

Online content

Any methods, additional references, Nature Research reporting summaries, source data, extended data, supplementary information, acknowledgements, peer review information; details of author contributions and competing interests; and statements of data and code availability are available at https://doi.org/10.1038/s41561-021-00695-3.

Received: 29 January 2020; Accepted: 19 January 2021;
Published online: 8 March 2021

References

1. Mahlstein, I., Knutti, S., Solomon, S. & Portmann, R. W. Early onset of significant local warming in low latitude countries. *Environ. Res. Lett.* **6**, 034009 (2011).
2. Coumou, D., Robinson, A. & Rahmstorf, S. Global increase in record-breaking monthly-mean temperatures. *Clim. Change* **118**, 771–782 (2013).
3. Hoegh-Guldberg, O. et al. in *Special Report on Global Warming of 1.5 °C* (eds Masson-Delmotte, V. et al.) Ch. 3 (IPCC, 2018).
4. *World Population Prospects 2019: Highlights* ST/ESA/SER.A/423 (United Nations, Department of Economic and Social Affairs, Population Division, 2019).
5. Vogel, M. et al. Regional amplification of projected changes in extreme temperatures strongly controlled by soil moisture–temperature feedbacks. *Geophys. Res. Lett.* **44**, 1511–1519 (2017).
6. Kovats, R. S. & Hajat, S. Heat stress and public health: a critical review. *Annu. Rev. Public Health* **29**, 41–55 (2008).
7. Mitchell, D. et al. Attributing human mortality during extreme heat waves to anthropogenic climate change. *Environ. Res. Lett.* **11**, 074006 (2016).
8. Hardy, J. D., Du Bois, E. F. & Soderstrom, G. F. Basal metabolism, radiation, convection and vaporization at temperatures of 22 to 35 °C. *J. Nutr.* **15**, 477–497 (1938).
9. Hardy, J. D. & Stolwijk, J. A. Partitional calorimetric studies of man during exposures to thermal transients. *J. Appl. Physiol.* **21**, 1799–1806 (1966).
10. Mora, C. et al. Global risk of deadly heat. *Nat. Clim. Change* **7**, 501–505 (2017).
11. Sherwood, S. C. How important is humidity in heat stress? *J. Geophys. Res. Atmos.* **123**, 808–810 (2018).
12. Delworth, T. L., Mahlman, J. D. & Knutson, T. R. Changes in heat index associated with CO_2-induced global warming. *Clim. Change* **43**, 369–386 (1999).
13. Willett, K. M. & Sherwood, S. Exceedance of heat index thresholds for 15 regions under a warming climate using the wet-bulb globe temperature. *Int. J. Climatol.* **32**, 161–177 (2012).
14. Fischer, E. M. & Knutti, R. Robust projections of combined humidity and temperature extremes. *Nat. Clim. Change* **3**, 126–130 (2013).
15. Coffel, E. D., Horton, R. M., Winter, J. M. & Mankin, J. S. Nonlinear increases in extreme temperatures paradoxically dampen increases in extreme humid-heat. *Environ. Res. Lett.* **14**, 084003 (2019).
16. Sherwood, S. C. & Huber, M. An adaptability limit to climate change due to heat stress. *Proc. Natl Acad. Sci. USA* **107**, 9552–9555 (2010).
17. *Ergonomics of the Thermal Environment—Assessment of Heat Stress Using the WBGT (Wet Bulb Globe Temperature) Index* ISO Standard No. 7243:2017 (International Organization for Standardization, 2017); https://www.iso.org/standard/67188.html
18. Byrne, M. P. & O'Gorman, P. A. Land–ocean warming contrast over a wide range of climates: convective quasi-equilibrium theory and idealized simulations. *J. Clim.* **26**, 4000–4016 (2013).
19. Byrne, M. P. & O'Gorman, P. A. Link between land–ocean warming contrast and surface relative humidities in simulations with coupled climate models. *Geophys. Res. Lett.* **40**, 5223–5227 (2013).
20. Byrne, M. P. & O'Gorman, P. A. Trends in continental temperature and humidity directly linked to ocean warming. *Proc. Natl Acad. Sci. USA* **115**, 4863–4868 (2018).
21. Zhang, Y. & Fueglistaler, S. How tropical convection couples high moist static energy over land and ocean. *Geophys. Res. Lett.* **47**, e2019GL086387 (2020).
22. Taylor, K. E., Stouffer, R. J. & Meehl, G. A. An overview of CMIP5 and the experiment design. *Bull. Am. Meteorol. Soc.* **93**, 485–498 (2012).
23. Sobel, A. H., Held, I. M. & Bretherton, C. S. The ENSO signal in tropical tropospheric temperature. *J. Clim.* **15**, 2702–2706 (2002).
24. Flannaghan, T. J. et al. Tropical temperature trends in Atmospheric General Circulation Model simulations and the impact of uncertainties in observed SSTs. *J. Geophys. Res.* **119**, 327–337 (2014).
25. Fueglistaler, S. Observational evidence for two modes of coupling between sea surface temperatures, tropospheric temperature profile and shortwave cloud radiative effect in the tropics. *Geophys. Res. Lett.* **46**, 9890–9898 (2019).
26. Pal, J. S. & Eltahir, E. A. B. Future temperature in southwest Asia projected to exceed a threshold for human adaptability. *Nat. Clim. Change* **6**, 197–200 (2016).
27. Im, E., Pal, J. S. & Eltahir, E. A. B. Deadly heat waves projected in the densely populated agricultural regions of South Asia. *Sci. Adv.* **3**, e1603322 (2017).
28. Dee, D. P. et al. The ERA-Interim reanalysis: configuration and performance of the data assimilation system. *Q. J. R. Meteorol. Soc.* **137**, 553–597 (2011).
29. Dunn, R. J. H., Willett, K. M., Parker, D. E. & Mitchell, L. Expanding HadISD: quality-controlled, sub-daily station data from 1931. *Geosci. Instrum. Methods Data Syst.* **5**, 473–491 (2016).
30. Rayner, N. A. et al. Global analyses of sea surface temperature, sea ice, and night marine air temperature since the late nineteenth century. *J. Geophys. Res. Atmos.* **108**, 4407 (2003).

Methods

Wet-bulb temperature. TW is thermodynamically defined as the temperature that an air parcel would have if cooled adiabatically to saturation at constant pressure by evaporation of water into it, all latent heat being supplied by the parcel. This process is enthalpy conserving; therefore, $c_pT+Lq=c_p\mathrm{TW}+Lq_{sat}(\mathrm{TW})$, where T and q are the temperature and the specific humidity of an environmental air parcel[31]. TW is empirically defined as the temperature read from the wet-bulb thermometer, which is a balance between diffusion of sensible heat from the environment to the saturated surface and the latent heat the other way around. Here we adopt the second definition because it is more relevant for the process of evaporative cooling of sweat. The two definitions give the same result due to the coincidence that the diffusivities of sensible and latent heat are the same. TW is calculated by solving the following equation using Newton's iteration: $c_pT+Lq=c_p\mathrm{TW}+\epsilon Le_{sat}(\mathrm{TW})/p_s$, where T, q and p_s are temperature, specific humidity and pressure of the surface air, ϵ is the molecular mass ratio of water vapour and air, e_{sat} is the saturation vapour pressure and L is the latent heat of condensation.

Wet-bulb globe temperature. WBGT evaluates the heat stress to which a person is exposed. It is used by workers, athletes and military. It is defined as $\mathrm{WBGT}=0.7\mathrm{TW}+0.3T_d$ (or $\mathrm{WBGT}=0.7\mathrm{TW}+0.2T_g+0.1T_d$ to take solar insolation into account), where TW is the wet-bulb temperature, T_g is the globe thermometer temperature and T_d is the dry-bulb temperature (or actual air temperature).

Station data. Station data from HadISD are selected on the basis of the following procedure. For each station, we first scan though TW measurements for each day and take only the daily averages of those days containing at least four measurements. Then, for the years containing more than 300 daily mean TWs, the annual-maximum TW is taken. In the end, stations with at least 20 valid annual-maximum TW values are included in this paper, which ends up to be 293 stations (Supplementary Fig. 8). For those stations, the average TW is subtracted within each station, then the anomalies are averaged among all stations as shown in Fig. 3.

Daily mean and 3-hourly TW from CMIP5 models. CMIP5 models provide surface air temperature and specific humidity on daily and 3-hourly frequency but not surface pressure. Therefore, we interpolate monthly surface pressure in a piece-wise manner to daily frequency for daily TW calculation and ignore the diurnal cycle in surface pressure for 3-hourly TW calculation. The error thus induced in TW is estimated to be less than 0.3 °C.

Data availability

CMIP5 model data provided by the World Climate Research Programme's Working Group on Coupled Modelling, and climate modelling groups can be accessed at https://esgf-node.llnl.gov/projects/cmip5. ERA-Interim data provided by European Centre for Medium-Range Weather Forecast (ECMWF) can be accessed at http://go.nature.com/3piVLPO. HadISD global sub-daily station dataset (v3.0.1.201909p) provided by Met Office Hadley Centre can be accessed at https://www.metoffice.gov.uk/hadobs/hadisd. HadISST data provided by the Met Office Hadley Centre can be accessed at https://www.metoffice.gov.uk/hadobs/hadisst.

Code availability

The computer code used in this paper is available from the corresponding author.

References

31. Iribarne, J. V. & Godson, W. L. in *Atmospheric Thermodynamics* Ch. 6 (Springer, 1973).

Acknowledgements

Y.Z. thanks J. Lin and G. Vecchi for suggestions on the manuscript. Y.Z. acknowledges support under award NA18OAR4320123 from the National Oceanic and Atmospheric Administration, US Department of Commerce (the statements, findings, conclusions, and recommendations are those of the author and do not necessarily reflect the views of the National Oceanic and Atmospheric Administration or the US Department of Commerce). S.F. acknowledges support from National Science Foundation under award AGS-1733818.

Author contributions

Y.Z. conceived the theory, performed the data analysis and wrote the manuscript. I.H. suggested the examination of observations/reanalysis. S.F. interpreted the widening of TW_{max} trend distribution in reanalysis (Fig. 3c). All authors discussed the results and edited the manuscript.

Competing interests

The authors declare no competing interests.

Additional information

Supplementary information The online version contains supplementary material available at https://doi.org/10.1038/s41561-021-00695-3.

Correspondence and requests for materials should be addressed to Y.Z.

Peer review information *Nature Geoscience* thanks the anonymous reviewers for their contribution to the peer review of this work. Primary Handling Editors: Tamara Goldin, Heike Langenberg, Tom Richardson.

Reprints and permissions information is available at www.nature.com/reprints.